Seismic data inversion with curvelet denoising preconditioning

V. M. Gomes* (GISIS/UFF), H. B. Santos (CEP/UNICAMP & INCT-GP), J. Schleicher (IMECC/UNICAMP & INCT-GP), A. Novais (IMECC/UNICAMP & INCT-GP), M. A. C. Santos (GISIS/UFF) and M. S. Q. Rocha (GISIS/UFF)

Abstract

Seismic inversion methods are highly sensitive to noise present in the data set. The need to enhance the signal-to-noise ratio (SNR) motivates many researchers do develop increasingly sophisticated denoising methods and combine them into other techniques. While some methodologies operate on a single scale, the curvelet transform established itself as multi-scale transform useful to decompose the seismic signals into multi-resolution elements. In this study, we evaluate the benefits of curvelet denoising as a preconditioning method for poststack seismic data in a 2D acoustic inversion process using a Bayesian framework. Our tests on a synthetic data set simulated in the Marmousi model, and a real data set from the Campos Basin offshore Brazil have shown that the curvelet thresholding method can be successfully applied for random noise elimination. Even the use of a hard global threshold might allow improvements in the deepest parts. Future work will have to show whether alternatives that ensure a more robust way of selecting the coefficients can take into account the wavelength change with depth.

Introduction

The aim of seismic inversion methods is to provide a subsurface model which is coherent with the recorded seismic data. Field data applications often face a problem with strong noise influence. The presence of noise brings instability to the seismic inverse problem and makes it hard to estimate a reliable acoustic impedance model, jeopardizing the estimation of the wavelet and even the impedance itself.

In the majority of denoising applications, we face the challenge of restoring the energy of the high-frequency part of the data without degrading the signal-to-noise (SN) ratio. This has motivated researchers to investigate sophisticated denoising techniques like the localized slant stack (McMechan, 1983), T-X prediction filtering (Abma and Claerbout, 1995), and the sparse transform-based method (Yuan et al., 2015) for random noise attenuation. Other techniques include the wavelet transform (Shan et al., 2009), which is able to detect local features in the time-frequency, and the S-transform adopted by (Parolai, 2009). All these techniques operate on a single scale.

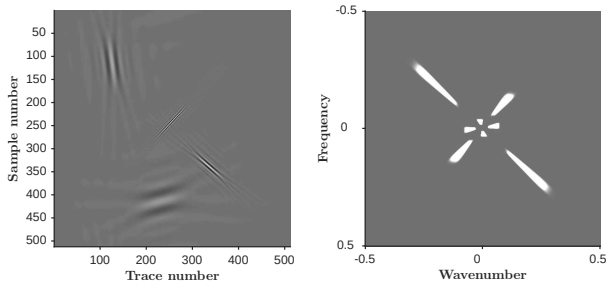

Figure 1: Four curvelets with different scale (left) and angles represented in both spatial- and frequency-wavenumber domains (right).

Candès and Donoho (2000) proposed the Curvelet Transform (CT), a new multi-scale transform that allows to decompose the seismic signals into multi-resolution elements. It acts in both the space-frequency domain and the angular orientation (Mallat, 1999). Moreover, the features of curvelet decomposition proved it to be an adequate tool for application in many steps of seismic data processing (Ma and Plonka, 2010). Some applications include the random-noise suppression by the combination of the thresholding method with a nonuniformly sampled curvelet transform (Hennenfent and Herrmann, 2006; Hennenfent et al., 2010), the application of the curvelet denoising method to 2D and 3D seismic data (Górszczyk et al., 2014; Neelamani et al., 2008), multiple attenuation (Herrmann and Hennenfent, 2008), and migration (Chauris and Nguyen, 2008).

In this work, we evaluate curvelet denoising as a preconditioning technique for poststack seismic data in an acoustic inversion process. We investigate its performance in noise suppression to a limit where visual and numerical artefacts become significantly dangerous to the data. It is to be noted that well-conditioned data guarantee faster convergence of the inversion. We study alternatives that allow to obtain better results from the inversion of data with significant noise. To perform our evaluation, we choose two examples: the synthetic Marmousi model (Versteeg, 1994) and a real dataset from the Marimba oil field in the Campos Basin offshore Brazil. Both analyses provide encouraging results.

Methodology

The proposed method consists of two main stages. During the first stage, preconditioning, we attempt to filter out unwanted information employing the curvelet denoising with a thresholding procedure. During the second stage, seismic data inversion, we try to achieve the same goal using a Bayesian acoustic poststack approach. In the next sections, we present a brief overview of the concepts.

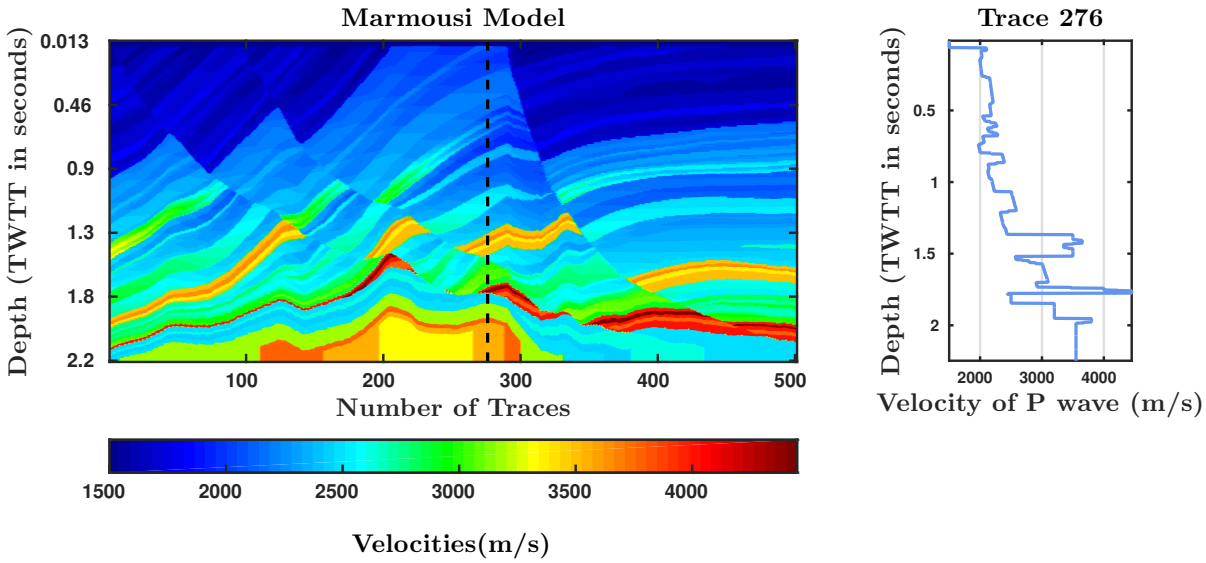

Figure 2: Marmousi P-velocity model and its 276th trace.

Curvelet denoising for seismic data

Seismic data are composed of reflections with considerable continuity across volume sections. Therefore, the reflections can be seen as geometric features, composed mostly, of line (2D) and surface (3D) singularities.

In denoising, the data are usually transformed to some sparse domain, and coefficients associated with noise are filtered out. Hence, for seismic purposes, transformation must assure the mentioned singularities are precisely reconstructed after coefficient filtering.

A well know sparsity-promoting transform is the Wavelet Transform (WT). However, even though it performs well for objects with point-like discontinuities, in 2D it fails for events with curve-like singularities, because of its isotropic elements. The Curvelet transform (CT) with highly directional-sensitivity and anisotropic elements (Ma and Plonka, 2010) can overcome this WT drawback.

The Curvelet transform was first presented in Candès and Donoho (2000). drawbacks in its algorithm discretization led to development of the second generation Discrete Curvelet transform (DCT) in Candès and Donoho (2003). This transform is a tight-frame capable of a near-optimal sparse representation of objects with discontinuities along smooth curve-like features by series expansion using needle-shaped elements.

Using indexes j for scale, k for rotation and $\boldsymbol{l} = (l_1, l_2) \in \mathbb{Z}^2$ for translation, curvelets can be defined for a continuous $\mathbb{R}^2$ space as a function of $\boldsymbol{x} = (x_1, x_2)$, by

$$\zeta_{j,k,l}(x) = \zeta_j(R_{\theta_{j,k}}(x - x_l^{(j,k)})). \tag{1}$$

Here, $R_{\theta_{j,k}}$ is the rotation matrix by angle $\theta_{j,k} = 2\pi k \cdot 2^{-\lfloor j/2 \rfloor}$ with $k \in \mathbb{N}_0$, and each spatial position $x_l^{(j,k)}$ is defined as $R_{\theta_{j,k}}^{-1}(l_1 2^{-j}, l_2 2^{-j/2})$. Therefore curvelets are obtained through anisotropic dilations, rotations and translations of a mother waveform, and the CT coefficients are the inner product of these curvelets and the data being analyzed.

Curvelets have compact support in the frequency domain and each one can be mapped to a localized polar wedge obeying the anisotropy scaling relation: length $\propto$ width^2. These wedges are functions of a pair of windows called $W(r)$ and $V(a)$, usually referred to as radial and angular windows, with $r \in (1/2, 2)$ and $a \in [-1, 1]$, through the relation:

$$U_j(r, \theta) = 2^{-3j/4} W(2^{-j} r) V\left(\frac{2^{-\lfloor j/2 \rfloor} \theta}{2\pi}\right), \tag{2}$$

with r and θ denoting polar coordinates in the frequency domain. Window $W(r)$ partitions the frequency domain into ring-shaped regions and $V(a)$ divides it into wedges, as exemplified in Figure 1.

Candès et al. (2006) showed a digital implementation of the second generation CT. For this purpose, they developed two new fast discrete curvelet transforms (FDCTs) via unequally spaced fast Fourier transform (USFFT) and via wrapping of specific Fourier samples.

In this work, we adopted the wrapping-based digital implementation of the FDCT because it represents a tight frame and is computationally faster than the USFFT-based one. To perform our numerical experiments, we use the software package CurveLab (Candès et al., 2006, available at http://www.curvelet.org), which contains the Matlab and C++ implementations of both the USFFT-based and the wrapping-based transforms.

We combine FDCT denoising with the method of Starck et al. (2002), which assumes the coefficients to be corrupted by additive noise. The procedure consists of calculating, from an initial noise estimate using Monte Carlo simulations, an approximate value for the noise amplitude (standard deviation $\tilde{\sigma}_k$ of the noise-corrupted data at each scale). At the next step, it applies an adaptive hard-thresholding rule to determine the reliable coefficients $\hat{y}_k$, which rise significantly above the noise level, as

$$\begin{cases} \hat{y}_k = y_k, & \text{if } |y_k| \geq \tau\tilde{\sigma}_k \\ \hat{y}_k = 0, & \text{if } |y_k| < \tau\tilde{\sigma}_k \end{cases}. \tag{3}$$

Table 1: Results from Marmousi test.

Threshold ($\times\sigma$)	PSNR		Error
	Value (dB)	Change	
5	24.59	+2.11	0.24
7.5	25.67	+3.25	0.14
10	26.23	+3.79	0.10
12	26.12	+3.70	0.07

Here τ represents the relative threshold value controlling how much information will be filtered out.

Poststack acoustic seismic inversion

A noteworthy problem of seismic inversion is the absence of low-frequency information in the seismic data. Pursuing a good initial model input as an a-priori constraint is a reasonable workaround to this barrier. In addition solving for a sparse spike-like reflectivity is an elegant mathematical solution to increase the bandwidth.

Within a Bayesian framework, both sparsity ensuring regularization norms (e.g. L1, Huber, Cauchy) and constraint dependence can be introduced to estimate a blocky impedance model (Ulrych and Sacchi, 2005). The objective function takes the form:

$$J = \kappa|r|_{L1} + \frac{1}{2}\|\frac{1}{\tilde{\sigma}}(Wr - s)\|^2 + \frac{1}{2}\|N^{-1}(Cr - B)\|^2, \quad (4)$$

where the first term is the sparsity norm (L1) of the reflectivity model (r), the second term is responsible for minimizing the misfit between observed (s) and calculated (Wr) data, and the last term constrains the model using the a-priori information.

In equation 4 above, κ ponders sparsity in the estimated reflectivity (r), $\tilde{\sigma}$ is an estimate of the noise level, W is the wavelet convolution matrix, C an integration operator and B is the natural logarithm of the normalized impedance. The term N is the diagonal matrix $N_{k,k} = \lambda_k$ responsible for constraining the solution, where λ is a vector of uncertainties of the a-priori information.

At last, it must be noted that the choice of both κ and σ, as well as the construction of the initial model, are initial steps in the inversion. Particular care has to be taken in these choices, because these parameters will define convergence to the global minimum of the objective function.

Applications

We test the proposed inversion with curvelet denoising preconditioning by applying it to synthetic and real data. Initial tests were performed considering pseudo-random white Gaussian noise (not shown here). Other tests were performed using data contaminated with colored Gaussian noise which has a higher influence on the low-frequency band of data (where inversion methods are more sensitive). Therefore, it is paramount for denoising techniques to be able to treat it.

To better understand the behavior of curvelet denoising, we evaluated errors with different standard deviations (σ), and thresholds were adaptively chosen with respect to the noise level. We used the peak signal-to-noise ratio (PSNR) and the L2-norm of the difference, respectively, to quantify the performance of the denoising and inversion in our approach.

Synthetic example - Marmousi model

As a first test, we applied the presented approach to a synthetic data from the Marmousi model (Versteeg, 1994), shown in Figure 2. The acoustic seismic volume was modeled using the convolutional model considering a Ricker wavelet with 20-Hz peak frequency.

To evaluate how denoising can influence inversion, we contaminated the data using three levels of colored random noise (σ = 10e-3, 20e-3, and 30e-3) and used relative threshold values of 5, 7.5, 10 and 12. The seismic data inversion uses an initial noise estimate of 5e-2 by means of the Bayesian acoustic poststack approach.

Table 1 summarizes the filtering and inversion results for all threshold values. The PSNR column is divided into two columns, one showing its value after denoising and the other (change) if it increased (positive) or decreased (negative) compared to the noisy data. The fourth column represents the error from inversion.

The results show that, up to a relative threshold of 10, an increase in the threshold leads to an increase in PSNR value, indicating that the lower coefficients carry predominantly noise. The behavior inverts when further increasing the threshold to 12. This can be attributed to the fact that filtering out more coefficients will possibly affect the ones associated with the most prominent reflections and certainly the localized high-amplitude anomalies, reducing the maximum dataset value and thus the PSNR. This filtering of information other than noise can be seen by the severe attenuation mostly of the shallower reflections considering a threshold of 12σ.

A drawback of curvelet denoising are linear events, not physically consistent, that can appear in the seismic section crossing the actual reflections. For an example, see the leftmost image in Figure 3. leftmost image) These events are characteristic of curvelet thresholding, representing weak-amplitude curvelets that emerge after inverse curvelet transform. They can be easily removed by directional control (i.e., filtering curvelets by dip).

The profiles in the right part of Figure 3 show the result of filtering with a threshold of 12σ for both noise levels. It is evident from this figure that the noise was not removed to guarantee a good visual quality even though relevant reflections can still be distinguished from noise. Moreover, small-amplitude reflections are hardly recovered, and close events (peaks and troughs in data) are not resolved, in the worst-case scenario being reconstructed as one.

Inversion results considering a noise level of σ = 20e-3 are shown in Figure 4. It can be noticed that denoising improves the inversion results. Moreover, it is difficult to decide which of the thresholds 10 or 12σ gives the best results. This indicates that both values are close to the optimum threshold, even though both lead, in general, to lower reflectivity values than the real model, probably due to a lack of low-frequency content in the data.

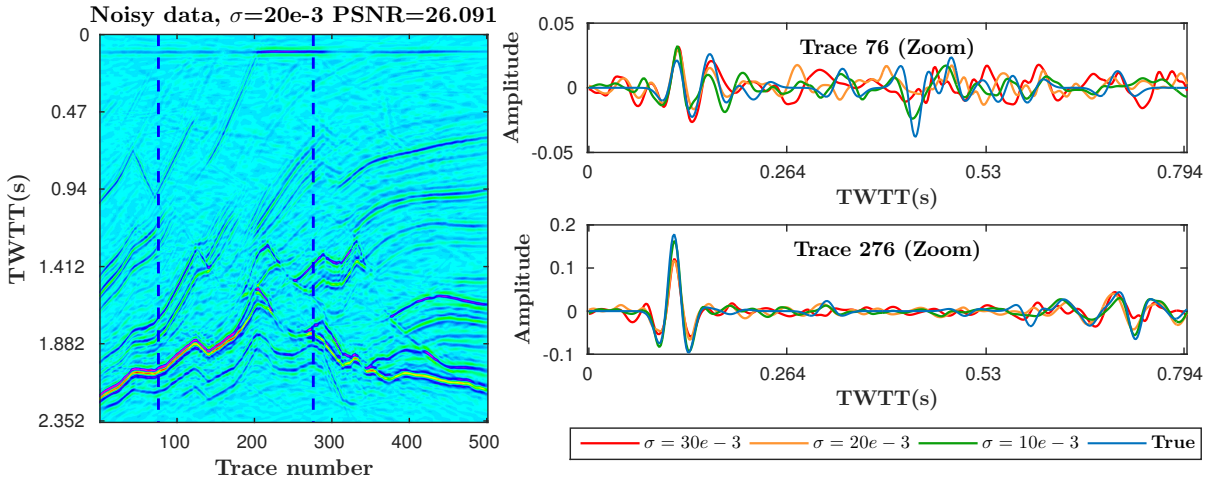

Figure 3: Denoising results considering a relative threshold of $\tau = 12$, i.e., accepting only coefficients with values of at least 12 times the noise level. The data were contaminated with a $\sigma = 20$e-3 noise.

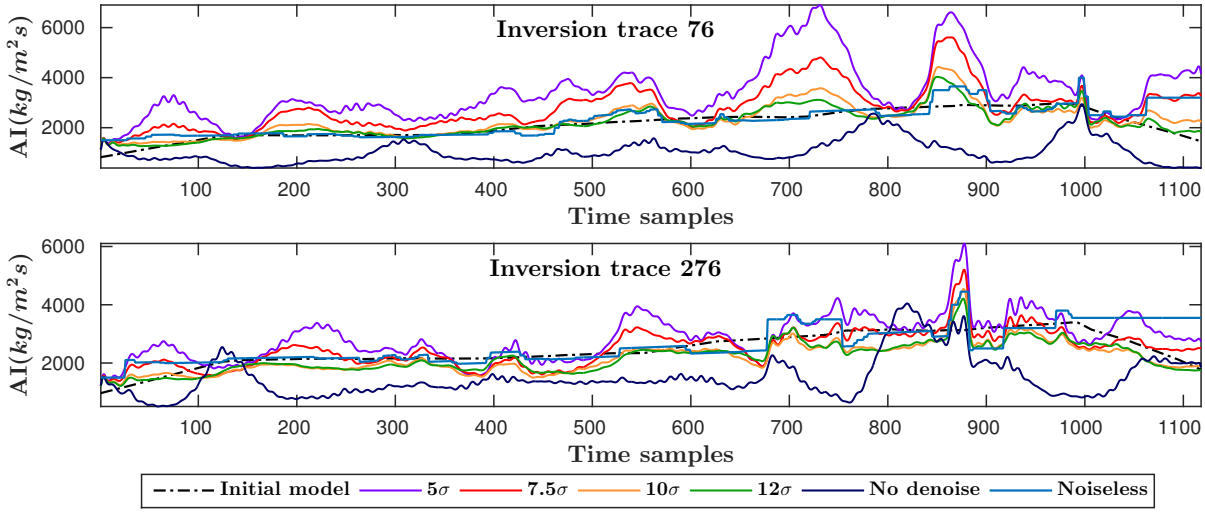

Figure 4: Inversion results for traces 76 and 276 for data contaminated with a $\sigma = 20$e-3 noise, and using all threshold values.

Applications to real data

We next applied our denoising technique to a real data set from the Marimba oil field in the Campos Basin offshore Brazil. Figure 5 shows a section of the seismic volume including a reservoir and additional information from three wells inside the volume, used for low-frequency model-building.

In the denoising analysis, we assumed four different noise intensities ($\sigma =$ 10e-3, 20e-3, 30e-3 and 50e-3). We used the same thresholds as in the synthetic case. Furthermore, the inversion analysis used both statistical and deterministic wavelets to understand better how denoising behaved in both scenarios and considered an initial noise estimate of 5e-4.

For a reference model, we used an inversion (indicated as HR inversion in Figure 7) from commercial software (HampsonRussell suite, CGG).

Table 2 shows the results for the real-data case with colored noise with $\sigma = 30$e-3. Its format is the same as the previous table except for the last two columns, associated with the inversion error for the two different wavelets.

Table 2: Results from real data tests (trace 156, inline 69).

Threshold ($\times\sigma$)	PSNR		Error Stat.	Error Deter.
	Value (dB)	Change		
5	28.98	+0.45	0.15	0.35
7.5	28.82	+0.29	0.11	0.26
10	28.41	-0.12	0.09	0.26
12	27.86	-0.67	0.10	0.24

Figure 6 exhibits similar features to the ones discussed in the previous section for the synthetic data, except for the linear artifacts. However, in the upper part of the section the amplitudes are somewhat attenuated, which makes the existing small faults difficult to observe.

The inversion analysis (Figure 7) shows that the results from the deterministic are stable as expected and do not vary much, while the statistical case allows for a better

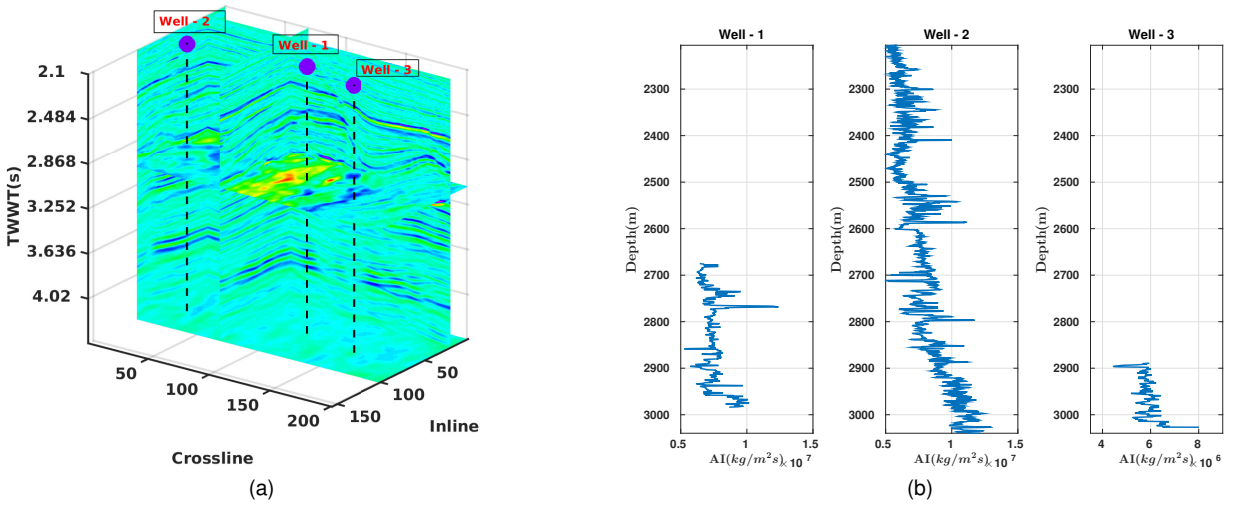

Figure 5: Seismic volume with log positions indicated and the acoustic impedance log for each well.

analysis of the denoising influence in the inversion. For the latter, as before, thresholds of $\tau = 10$ and 12 yielded the best results, closer to the reference model (HR inversion).

Conclusions

We investigated the benefits of curvelet denoising together with an adaptive hard-thresholding rule as a preconditioning method to poststack seismic data in an acoustic inversion procedure. To evaluate if the curvelet denoising was able to increase the resolution without degrading the SNR, two data sets were contaminated with white and colored noise for different signal-to-noise ratios, being the highest values of noise uncommon in a pre-processed seismic data.

The tests, performed on synthetic data from the Marmousi model and a real data set from the Marimba oil field in the Campos Basin offshore Brazil, led to similar conclusions. The methodology clearly increased the SNR. The quality of the achieved improvements depended on the choice of the coefficients.

Because our filtering is based on a global threshold assumption, the increment in the wavelength with depth is not considered. The decreasing of the SNR in shallower parts of the model is a consequence of the application of a hard threshold value, which was used in an attempt to achieve improvements in deeper parts.

Future investigations will have to find alternative strategies of filtering that are capable of reducing the noise of the coefficients in an efficient manner so that coefficients associated with events of lower energy are not filtered with the same threshold as coefficients associated with higher energy. Furthermore, the methodology provided encouraging results to justify evaluating it in a seismic inversion of prestack seismic data, e.g., amplitude variation with offset and full-waveform inversion.

Acknowledgments

We thank the Curvelet.org team for providing the CurveLab toolbox, and ANP for allowing the use of the data from its database. The first author thanks the GISIS (Grupo de Imageamento Sísmico e Inversão Sísmica) at UFF for allowing the use of its laboratories during the tests. He is also grateful to CGG for providing through UFF the HampsonRussell software for inversion. H. B. Santos is grateful to Petrobras, ANP and PRH-PB230 for his fellowships. This research was supported by the Brazilian research agencies CAPES, CNPq, FAPESP and FINEP. Additional support for the authors was provided by the sponsors of the *Wave Inversion Technology (WIT) Consortium*, Hamburg, Germany.

References

Abma, R., and J. Claerbout, 1995, Lateral prediction for noise attenuation by t-x and f-x techniques: Geophysics, **60**, 1887–1896.

Candès, E. J., L. Demanet, D. Donoho, and L. Ying, 2006, Fast discrete curvelet transforms: Multiscale Modeling & Simulation, **5**, 861–899.

Candès, E. J., and D. L. Donoho, 2000, Curvelets: A surprisingly effective nonadaptive representation for objects with edges: Technical Report No. 28, Stanford University.

———, 2003, New tight frames of curvelets and optimal representations of objects with piecewise C^2 singularities: Communications on Pure and Applied Mathematics, **57**, 219–266.

Chauris, H., and T. Nguyen, 2008, Seismic demigration/migration in the curvelet domain: Geophysics, **73**, S35–S46.

Górszczyk, A., A. Adamczyk, and M. Malinowski, 2014, Application of curvelet denoising to 2D and 3D seismic data — practical considerations: Journal of Applied Geophysics, **105**, 78–94.

Hennenfent, G., L. Fenelon, and F. J. Herrmann, 2010, Nonequispaced curvelet transform for seismic data reconstruction: A sparsity-promoting approach: Geophysics, **75**, WB203–WB210.

Hennenfent, G., and F. Herrmann, 2006, Seismic denoising with nonuniformly sampled curvelets: Computing in Science & Engineering, **8**, 16–25.

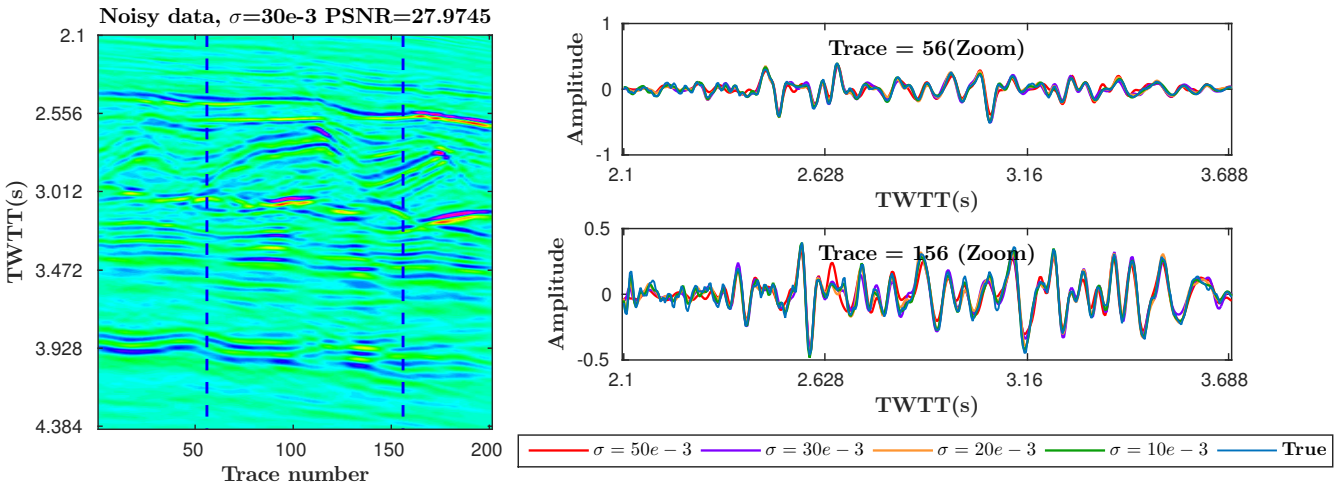

Figure 6: Denoising results considering a threshold of 12 times the noise level, considering data contaminated with noise with σ = 30e-3, using all thresholds.

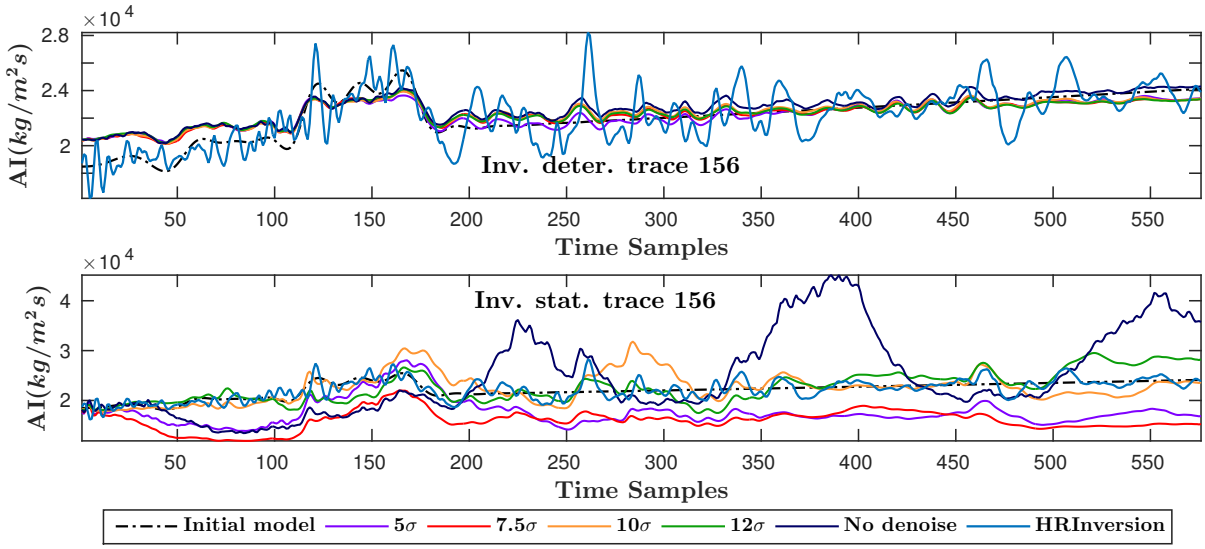

Figure 7: Inversion results considering a threshold of 12 times the noise level considering data contaminated with a σ = 20e-3 noise using all thresholds.

Herrmann, F. J., and G. Hennenfent, 2008, Non-parametric seismic data recovery with curvelet frames: Geophysical Journal International, **173**, 233–248.

Ma, J., and G. Plonka, 2010, The curvelet transform: IEEE Signal Processing Magazine, **27**, 118–133.

Mallat, S., 1999, A wavelet tour of signal processing, second edition (wavelet analysis & its applications): Academic Press.

McMechan, G. A., 1983, p-x imaging by localized slant stacks of t-x data: Geophysical Journal International, **72**, 213–221.

Neelamani, R., A. I. Baumstein, D. G. Gillard, M. T. Hadidi, and W. L. Soroka, 2008, Coherent and random noise attenuation using the curvelet transform: The Leading Edge, **27**, 240–248.

Parolai, S., 2009, Denoising of seismograms using the S transform: Bulletin of the Seismological Society of America, **99**, 226–234.

Shan, H., J. Ma, and H. Yang, 2009, Comparisons of wavelets, contourlets and curvelets in seismic denoising: Journal of Applied Geophysics, **69**, 103–115.

Starck, J.-L., E. J. Candès, and D. L. Donoho, 2002, The curvelet transform for image denoising: IEEE Transactions on image processing, **11**, 670–684.

Ulrych, T. J., and M. D. Sacchi, 2005, Information-based inversion and processing with applications: Elsevier, **36**, 1–436.

Versteeg, R., 1994, The marmousi experience: Velocity model determination on a synthetic complex data set: The Leading Edge, **13**, 927–936.

Yuan, S., S. Wang, C. Luo, and Y. He, 2015, Simultaneous multitrace impedance inversion with transform-domain sparsity promotion: Geophysics, **80**, R71–R80.